

MINERALOGY AND PROVENANCE OF CLAYS IN MIAROLITIC CAVITIES OF THE PIKES PEAK BATHOLITH, COLORADO

DANIEL E. KILE[§]

U.S. Geological Survey, 3215 Marine Street, Suite E-127, Boulder, Colorado, 80303, U.S.A.

ABSTRACT

Clay samples from 105 cavities within miarolitic granitic pegmatites throughout the Pikes Peak batholith, in Colorado, were analyzed by powder X-ray diffraction (XRD). Smectite (beidellite), illite, and kaolinite were found within the cavities. Calculation of crystallite-thickness distribution (CTD), mean thickness of the crystallites, and variance in crystallite thickness, as deduced from XRD patterns, allowed a determination of provenance and mode of formation for illite and smectite. Authigenic miarolitic-cavity illite and smectite show lognormal CTDs and larger mean thicknesses of crystallites than do their soil-derived counterparts; non-lognormal illite in a cavity results from mixing of cavity and soil illite. Analysis of mean thickness and thickness variance shows that crystal growth of illite is initiated by a nucleation event of short duration, followed by surface-controlled kinetics. Crystallization of the miarolitic cavity clays is presumed to occur by neof ormation from hydrothermal fluids. The assessment of provenance allows a determination of regional and local distributions of clay minerals in miarolitic cavities within the Pikes Peak batholith.

Keywords: smectite, illite, kaolinite, miarolitic cavity, crystallite-thickness distribution, crystallite-thickness variance, granitic pegmatite, clay minerals, Pikes Peak batholith, Colorado.

SOMMAIRE

Des échantillons provenant de 105 cavités dans des filons de pegmatite miarolitique granitique de part et d'autre du batholite de Pikes Peak, au Colorado, ont été analysés par diffraction X (méthode des poudres). Smectite (beidellite), illite, et kaolinite sont présentes dans ces cavités. Un calcul de la distribution de l'épaisseur des cristallites, de leur épaisseur moyenne, et de la variance de leur épaisseur permet de déterminer la provenance et le mode de formation de l'illite et de la smectite. L'illite et la smectite authigènes des cavités miarolitiques font preuve d'une distribution log-normale de l'épaisseur des cristallites, et une épaisseur supérieure par rapport à leur homologues dérivés des sols; l'illite des cavités ayant une distribution non log-normale des épaisseurs résulterait d'un mélange d'illite formée dans la cavité et d'illite dérivée de sols. Une analyse des épaisseurs moyennes et de la variance des épaisseurs montre que la croissance de l'illite a été initiée par un événement bref causant la nucléation, suivi d'un épisode où la cinétique était régie par les surfaces. La cristallisation des argiles dans les cavités miarolitiques résulterait d'une néoformation aux dépens d'une phase fluide hydrothermale. L'évaluation de provenance permet une détermination des distributions régionale et locale des minéraux argileux dans les cavités miarolitiques au sein du batholite de Pikes Peak.

(Traduit par la Rédaction)

Mots-clés: smectite, illite, kaolinite, cavité miarolitique, distribution de l'épaisseur des cristallites, variance de l'épaisseur des cristallites, pegmatite granitique, minéraux du groupe des argiles, batholite de Pikes Peak, Colorado.

INTRODUCTION

The Pikes Peak batholith (PPB) in central Colorado is world-renowned for hosting a variety of euhedral minerals in pegmatites, including the amazonitic variety of microcline and associated smoky quartz. Although numerous studies have documented the identity and paragenesis of such minerals within miarolitic cavities in the Pikes Peak batholith (*e.g.*, Foord & Martin

1979, Foord *et al.* 1995, Kile & Foord 1998, Kile & Eberl 1999), none has addressed the formation of clay minerals during the last stages of crystallization in these cavities. Foord *et al.* (1986) provided a detailed study of clays found in crystal-bearing cavities in pegmatites in San Diego County, California; no published studies have appeared on the cavity clays in the PPB. Accordingly, in this paper an inventory of the clay minerals found in miarolitic cavities is presented, along with

[§] *E-mail address:* dkile4@comcast.net

their distribution throughout the PPB based on results of X-ray-diffraction analysis of 105 samples.

BACKGROUND INFORMATION

A study of clay minerals in miarolitic cavities (in some cases referred to as "pockets") is necessarily complicated because clays can be formed either through hydrothermal crystallization or by weathering processes. Early investigators presumed that pocket clays result from weathering, either from decomposition of dike minerals or the surrounding rock (*e.g.*, Schaller 1925, Laudermilk & Woodford 1934), whereas later investigators postulated both hypogene (*i.e.*, by hydrothermal action) and supergene (*i.e.*, by weathering processes) origins for such clays (*e.g.*, Jahns & Wright 1951, Foord *et al.* 1986). Determination of provenance is difficult at best, with earlier investigators relying mostly on indirect evidence, *e.g.*, proximity to surface and extent of weathering, association with sulfides, color, *etc.* In the PPB, the problem is compounded by the fact that many miarolitic cavities are near the surface and largely disintegrated, with soil-derived clays having infiltrated the disrupted cavity. However, recent development of computer programs to analyze crystallite thickness-distributions (CTDs) based on X-ray-diffraction (XRD) data have provided a means of assessing the provenance of clays within miarolitic cavities.

LOCATION AND GEOLOGY

The PPB is a Precambrian, anorogenic, epizonal batholith that is exposed in central Colorado over an area of about 5000 km². Numerous younger intrusive bodies (late-stage variants of the PPB) of sodic or potassic affinity are located throughout the batholith. Emplacement of these plutons and consequent fracturing of the host granite localized the formation of miarolitic pegmatites to areas within or adjacent to the intrusive bodies. The pegmatite areas that host miarolitic cavities are most prevalent in the southern part of the PPB; these are remarkable for their euhedral specimens of the amazonitic variety of microcline, smoky quartz, goethite, topaz, fluorite, among other minerals, which occur in well-known localities such as Glen Cove, Spruce Grove Campground, Devils Head, Wigwam Creek, and Crystal Park, and the Crystal Peak and Lake George areas (Fig. 1). The latter two localities are associated with the Lake George ring complex (LGR), one of the largest and mineralogically most important of the late intrusive bodies. It is a composite structure composed of a sequential series of intrusions with a syenite core, surrounded by fine- to medium-grained granitic rock units. Differential weathering has produced a topographically concentric structure in this ring complex. The largest of the late intrusive bodies is the Redskin stock, which is enriched in Li, Be, and Sn, and hosts topaz-bearing pegmatites as well as Be-

rich greisen deposits (Hawley 1969, Hawley & Wobus 1977, Desborough *et al.* 1980). Additional details of the PPB are given in Hawley & Wobus (1977), Wobus & Anderson (1978), Wobus (1986), and Hutchinson (1976, 1988).

Miarolitic pegmatites typically consist of an outer graphic zone, and commonly contain a centrally located cavity. Miarolitic cavities in the PPB range in size from centimeters to meters in length; they usually show at least a moderate degree of disintegration, either by tectonic activity or by weathering, which results in detachment of the minerals from cavity walls (see Kile & Foord 1998). The cavities are usually partly or completely filled by clay minerals (Fig. 2), which enclose fragments of minerals and pegmatite in a random jumble. The clays are usually impregnated with and colored by various Fe-oxides and hydroxides, imparting a red, brown or reddish orange color.

Early crystallization within miarolitic cavities is hypothesized to occur under magmatic conditions from an exsolved aqueous vapor phase (Kile & Foord 1998, and references therein). Continued cooling of the host rock, depletion of aqueous silica, and a corresponding reduction in pressure and temperature gradually lead to hydrothermal, hypogene crystallization, wherein low-temperature minerals, including clays, are presumed to crystallize (Foord *et al.* 1986). Additional details of cavity paragenesis and morphology were given in Kile & Foord (1998).

METHODS

One hundred and five samples of clay were collected from miarolitic cavities at various localities throughout the PPB; many of these clays show a heterogeneous mixture of clay species, as well as mixed-layering effects which, as discussed below, render them unsuitable for further analyses. Accordingly, to avoid ambiguity in interpreting results, only those samples of miarolitic cavities showing a dominant clay phase were tabulated and further analyzed. Moreover, only samples showing a distinct, symmetrical 001 peak in powder diffractograms are suitable for assessment of CTD and mean thickness of crystallites, as discussed below. Thus on a basis of the above criteria, of the original 105 samples, 59 were selected for further study; these are presented in Table 1.

Clays were collected primarily as surface coatings adhering to macroscopic minerals within miarolitic cavities, with the assumption that such material would more likely represent authigenic clays. Most of the miarolitic cavities show some degree of weathering and disintegration, with presumed subsequent infiltration by soil-derived clays; accordingly, soil samples were collected and analyzed from eight representative localities in the PPB to provide a basis for comparison with cavity clays and to permit distinction between soil-derived and authigenic clay minerals. Soil samples

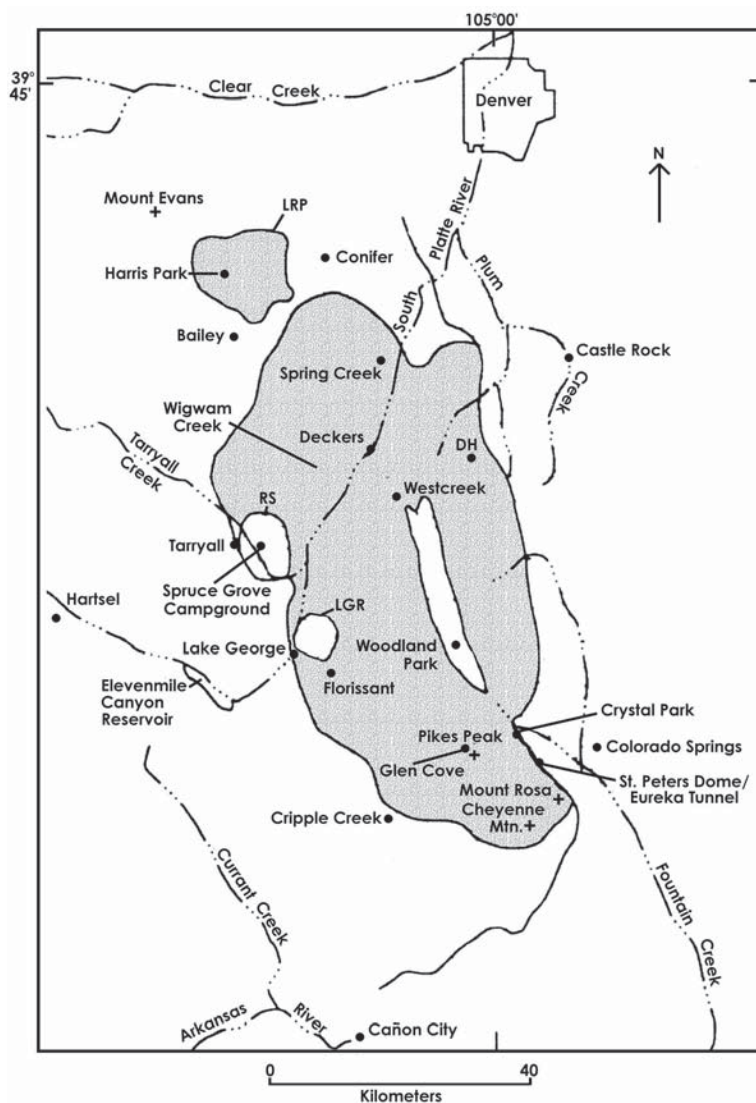


FIG. 1. Geological index map of the Pikes Peak batholith (shaded areas) showing locations of major late-stage potassic plutons and other geographic features. LGR: Lake George ring complex, RS: Redskin stock, DH: Devils Head, LRP: Lone Rock pluton. Map adapted from Foord *et al.* (1995).

were collected from a depth of 15–30 cm, at a point of transition between the soil horizon and relatively unweathered granitic rock. A list of soil samples is presented in Table 2.

Samples were prepared for XRD analysis by ultrasonic dispersion of approximately 50 mg of sample in 2 mL water and settling to remove the majority of non-clay minerals, followed by air-drying on a glass slide and ethylene glycol saturation for 48–72 h in a desiccator.

Diffractograms were acquired with a Siemens D-500 diffractometer using a Cu-radiation source (operating at 40 kV, 30 mA), a scintillation detector, and a graphite monochromator. Detector slits were set at 1°, with a 2.3° Soller slit between the X-ray tube and the detector. Scans were run in step mode from 2 to 65° 2 θ , with 2 seconds/step, and 0.02° 2 θ per step. Clay minerals were identified based on 001 reflections as given in standard tables.

TABLE 1. INVENTORY OF SELECTED CLAY SAMPLES FROM MIAROLITIC CAVITIES, PIKES PEAK BATHOLITH, COLORADO

Sample number	Locality	Mean thickness, nm	α	β^2	d^*	CTD shape	Sample number	Locality	Mean thickness, nm	α	β^2	d^*	CTD shape
Smectite							Illite						
PP EG4	Ypc, N LGR	5.7	1.63	0.19	16.81	-LN	PVP-1	Ypf, SW LGR	8.9	2.21	0.25	9.99	LN
PP EG9	Ypc, N LGR	6.4	1.74	0.23	16.36	-LN	PP EG2	Ypm, SW LGR	6.1	1.68	0.31	9.99	-LN
PP EG10	Wigwam Cr./SP	7.0	1.82	0.24	16.35	-LN	PVP-8	Ypc, N of LGR	12.7	2.32	0.41	9.98	Asy.
PP EG13	Ypc, N LGR	7.3	1.85	0.25	16.51	-LN	PVP-15	Devils Head	9.8	2.25	0.21	10.04	LN
PP EG18	Ypc, N LGR	5.8	1.62	0.18	17.14	-LN	PVP-20	Ypf, SW LGR	7.3	2.01	0.39	16.51	Asy.
PP EG24 ^f	Ypm, N LGR	6.6	1.76	0.22	16.81	-LN	PVP-27	Ypm, SW LGR	8.3	2.00	0.24	9.98	-LN
PP EG25	Ypc, N LGR	6.0	1.69	0.20	16.81	-LN	PVP-31	Ypf, SW LGR	9.0	2.17	0.29	9.98	LN
PP EG33 ^g	Ypm, N LGR	7.3	1.86	0.22	16.66	LN	PVP-32	Wigwam Cr./SP	7.6	2.05	0.28	9.98	LN
PP EG40	Ypc, NE LGR	6.2	1.69	0.22	16.50	-LN	PPG EG43	Ypc, N LGR	6.7	1.76	0.34	9.99	-LN
PP EG46	Ypc, N LGR	6.2	1.70	0.21	16.51	-LN	PVP-44	Ypc, N LGR	8.1	2.06	0.28	10.03	LN
PP EG48 ^h	Wigwam Cr./TH	7.1	1.82	0.25	16.50	-LN	PPG EG65	Ypc, N LGR	6.7	1.67	0.34	10.03	-LN
PP EG59	Ypc, N LGR	6.4	1.73	0.24	16.66	-LN	PVP-71	Ypc, N LGR	8.1	2.10	0.30	9.99	-LN
PP EG62	Wigwam Cr./SP	7.0	1.83	0.23	16.50	-LN	PPG EG81	Ypc, N LGR	7.3	1.85	0.31	10.03	-LN
PP EG68	Ysg, N LGR	7.2	1.84	0.24	16.82	-LN	PVP-85 [†]	Devils Head	9.0	2.20	0.19	10.10	LN
PPG EG72 ^g	Ypm, N LGR	7.3	1.88	0.23	16.81	LN	PVP-92	Ypc, N LGR	8.7	2.16	0.22	10.09	-LN
PP EG74 ^g	Ypc, N LGR	8.2	1.98	0.25	16.66	LN	PVP-100	Ypc, N LGR	7.4	2.04	0.28	9.99	-LN
PPG EG77	Ypm, NE LGR	5.3	1.56	0.20	16.82	-LN	PVP-105	Ypf, E LGR	9.3	2.25	0.30	10.04	-LN
PP EG82	Ypm, NE LGR	5.7	1.66	0.17	16.82	-LN	PPG EG112	Ypc, NE LGR	7.3	1.88	0.35	10.04	-LN
PPG EG90 ^g	Ypc, N LGR	8.0	1.95	0.26	16.67	LN	Kaolinite						
PPG EG 93 ^g	Ysg, N LGR	7.3	1.87	0.23	16.81	-LN	PP EG22b	Harris Park	~15	1.96	0.70	7.13	-LN
PPG EG99	Ypc, E LGR	6.0	1.70	0.19	16.82	-LN	PPG EG53	Ypm, SW LGR	6.7	1.34	1.05	7.13	-LN
PPG EG101	Ypm, NE LGR	5.4	1.57	0.19	16.81	-LN	PPG EG85 [†]	Devils Head	18.4	2.73	0.36	7.14	-LN
PPG EG103 ^g	Ypc, N LGR	8.1	1.93	0.28	16.82	-LN	PPG EG89	St. Peter's Dome	4.6	1.28	0.47	7.19	-LN
PP EG104 ^h	Ypc, N LGR	7.7	1.89	0.26	16.82	-LN	PP EG91	Eureka tunnel	25.6	3.11	0.27	7.14	-LN
PP EG106	Ypc, N LGR	6.4	1.73	0.24	16.51	-LN	PPG EG124	RSG, Spruce Grove Camp-ground	8.8	1.78	0.74	7.14	-LN
PPG EG107 ^g	Ypc, N LGR	7.4	1.85	0.28	16.82	-LN	PPG EG126	Wigwam Cr./TH	n.d. [§]	n.d. [§]	n.d. [§]	7.07	n.d. [§]
PP EG108	Ypc, N LGR	6.7	1.76	0.26	16.98	-LN	PPG EG127	Wigwam Cr./TH	22.7	3.00	0.33	7.14	-LN
PPG EG109	Ypc, N of LGR	5.7	1.62	0.20	16.81	-LN	PPG 135	Sentinel Rock	23.9	3.08	0.19	7.20	-LN
PPG EG110	Ypc, N of LGR	5.4	1.56	0.19	16.82	-LN							
PP EG113	Ypc, N LGR	6.0	1.67	0.21	16.97	-LN							
PP EG116	Ypc, N LGR	6.3	1.72	0.22	16.52	-LN							
PPG EG119	Ypc, N of LGR	5.3	1.54	0.18	16.98	-LN							

Note that the overlapping samples on map (Fig. 15) are shown as one point. α : natural logarithm of crystallite thickness; β^2 : variance of the natural logarithm of crystallite thickness. [§] Not determined because of asymmetrical peak. n.d.: not determined. [†] Sample contains illite and kaolinite, both of which were studied. * The d -value is derived from the XRD pattern of the ethylene-glycol-treated sample. ^h Determined to be principally beidellite. LN: lognormal crystallite-thickness distribution (CTD), -LN: approximately lognormal CTD, Asy.: asymptotic CTD, -LN: CTD is not lognormal. TH: trailhead locality at Wigwam Creek, SP: Sugarloaf Peak locality at Wigwam Creek, Ypc: coarse-grained granite, Ypm: medium-grained granite, Ypf: fine-grained granite, LGR: Lake George ring complex, RSG: Redskin Granite.

Selected illite-bearing samples were further size-separated to a <2- μ m fraction, Na-saturated, and treated with polyvinylpyrrolidone (PVP) to allow determination of CTD of the fundamental illite crystallites based on the Bertaut-Warren-Averbach (BWA) method and using the MudMaster computer program (Eberl *et al.* 1996, 1998a) to analyze the shape of the 001 peak. This procedure entails correction for the combined broadening effects of Lorentz polarization function (L_p) and the layer-scattering intensity (G^2) followed by Fourier analysis of the interference function (by the BWA method) to calculate the distribution of thicknesses of X-ray scattering domains. This analysis gives the shape of the thickness distribution (*i.e.*, CTD), which can be described by two parameters, the mean of the natural logarithms of crystallite thicknesses (α), and the variance of the natural logarithms of thicknesses

(β^2). Determination of the shape of the CTD was based on comparison of an experimental curve with that of a theoretical lognormal curve generated by the MudMaster program; the shape of plots was designated as lognormal (*i.e.*, logarithms of the crystallite thicknesses are lognormally distributed), near-lognormal (closely matches the theoretical curve with only minor deviation), non-lognormal (negligible fit to theoretical curve), or asymptotic (size frequencies are greatest in the smallest size-classes). The degree of fit to a theoretical lognormal curve was done by visual estimate; statistical analysis cannot be employed because only size frequencies are derived from XRD data, whereas statistical tests such as chi-square or Kolmogorov-Smirnov require numbers of crystals.

Selected smectite-bearing samples were similarly processed, being Na-saturated and glycolated (rather



FIG. 2. Close-up view of the interior of a miarolitic cavity showing detached crystals of amazonitic microcline and smoky quartz, partly enclosed by pocket clay containing broken shards of crystals and pegmatite wallrock. The field of view is approximately 30 cm across.

than PVP treatment, which causes the smectite reflections to disappear), and then analyzed to determine values of CTD. Only those samples with high expandability (*i.e.*, relatively pure smectite with a minimal mixed-layer structure and distinct and symmetrical peaks) were used for this analysis, as peak broadening can be related to either crystallite thickness or to interlayering; valid results by the BWA method cannot be obtained from mixed-layer clays.

In addition, ten smectite-rich clays were analyzed for the presence of a dioctahedral or trioctahedral structure by evaluating the d value of the 060 reflection from a random mount of the $<2\text{-}\mu\text{m}$ size fraction (Brindley 1980); further differentiation between beidellite and montmorillonite was done by the Greene–Kelley test (Starkey *et al.* 1984), whereby the sample is Li-saturated, heated to 250°C overnight, glycolated, and X-rayed in an oriented mount. Estimates of percent expandability for smectite-group phases were based on the amount of low-angle scattering in the 2 to 8° 2 θ region (Reynolds 1980); calculation of expandability based on the positions of second- and third-order peaks in glycol-solvated samples proved to be inconsistent, likely a result of the low intensities of those peaks.

CLAY MINERALOGY AND ASSESSMENT OF PROVENANCE

Clays within the miarolitic cavities show a varied mineralogy, and principally consist of smectite, illite and kaolinite. Much of the clay within the miarolitic

TABLE 2. INVENTORY OF SELECTED BACKGROUND (SOIL) CLAY SAMPLES FROM THE PIKES PEAK BATHOLITH, COLORADO

Sample number	Locality	Mean thickness, nm	α	β^2	d^*	CTD shape
Smectite						
BKG-3	Ysg, LGR	6.2	1.69	0.23	16.36	≠ LN
BKG-4	Ypm, LGR	n.d.	n.d.	n.d.	n.d.	n.d.
Illite						
BKGPVP-1	Ypc, N LGR	6.2	1.53	0.57	10.07	Asy.
BKGPVP-2	Ypc, N LGR	5.4	1.44	0.45	9.96	Asy.
BKGPVP-3	Ysg, N LGR	5.4	1.39	0.50	10.07	Asy.
BKGPVP-4	Ypm, LGR	6.9	1.62	0.59	10.09	Asy.
BKGPVP-5	Ypf, SW LGR	5.6	1.43	0.52	10.12	Asy.
BKGPVP-6	RSG, Spruce Grove Camp-ground	5.9	1.47	0.55	10.05	Asy.
BKGPVP-7	Ypc, N LGR	5.3	1.38	0.53	9.98	Asy.
BKG-8	Spring Creek	n.d.	n.d.	n.d.	10.16	n.d.

N LGR: northern Lake George ring complex, SW LGR: southwestern Lake George ring complex, RSG: Redskin Granite, Ypc: coarse-grained granite, Ypm: medium-grained granite, Ypf: fine-grained granite, Ysg: syenite.

* d value from XRD pattern of ethylene-glycol-treated sample, α : natural logarithm of crystallite thickness; β^2 : variance of the natural logarithm of crystallite thickness. Asy.: asymptotic crystallite-thickness distribution (CTD), ≠LN: CTD not lognormal, n.d.: not determined.

cavities is considered authigenic (*i.e.*, having formed by hydrothermal or hypogene processes within the cavity), but given the extent of cavity disruption, it also is likely that some of the clay is allochthonous,

having infiltrated from the surrounding soils that were derived from decomposed granitic rocks. These clays, formed by diagenetic and weathering processes, similarly contain mixtures of smectite, illite, and kaolinite; however, only illite was consistently found to be present in the soils. Analysis of the shapes of the CTD proved useful for assessing the provenance of clays within the miarolitic cavities. In Tables 1 and 2, the data for both miarolitic cavity and soil clays are summarized. Criteria for distinguishing authigenic from allochthonous clays are discussed below.

Smectite

Smectite is present in both miarolitic cavities and in soils, but smectite from miarolitic cavities (*e.g.*, from northern areas of the LGR, in both coarse- and medium-grained granite, and from Sugarloaf Mountain near Wigwam Creek) shows a high percent (~85–100%) expandability, and most samples show a lognormal or close to lognormal CTD (*e.g.*, Figs. 3 and 4). In contrast, seven of the eight soil samples collected (these seven were from areas of coarse-, medium-, and fine-grained granitic rocks and include the above localities from the LGR and Wigwam Creek) show a relatively low degree of expandability (*e.g.*, Fig. 5) based on the low relative valley-to-peak intensity of the 001 reflection (Reynolds 1980). Only one sample of soil, collected from above a quartz syenite in the LGR (sample BKG-3), shows a comparatively high-expandability smectite with a symmetrical 001 peak; however, compared to most of the samples from miarolitic cavities, this sample proved to have a distinctly non-lognormal CTD (Fig. 6).

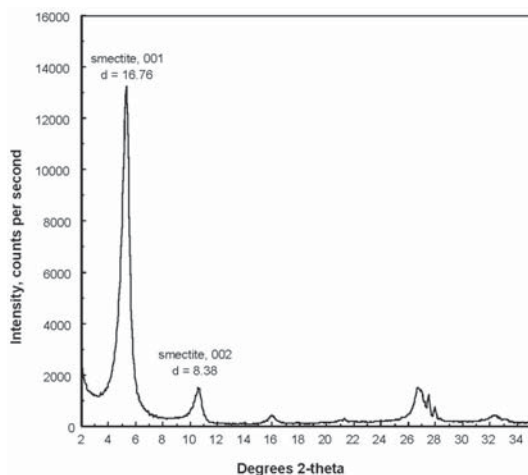


FIG. 3. XRD pattern of a glycolated, highly expandable smectite (beidellite) from a miarolitic cavity in the LGR (sample no. 74).

The mixed layering effects of clays seen in soil samples derived from granitic rocks, manifested by peak broadening and non-lognormal CTD, are presumed to be related to weathering processes. In contrast, clay samples showing a high expandability and lognormal CTD are presumed to have formed *in situ* by hydrothermal or hypogene processes. Furthermore, smectite clays from miarolitic cavities showing a lognormal CTD have distinctly larger mean thickness of crystallites (α) than do non-lognormal samples from miarolitic cavities and soil clay samples (Fig. 7). Accordingly, miarolitic cavity samples (particularly those within granitic rocks) showing a substantial proportion of low-expandability, mixed-layer clays are inferred to reflect infiltration of allochthonous soil-derived clay.

Six samples of miarolitic cavity clay containing a highly expandable smectite were found to be dioctahedral, with d_{060} values of 1.49–1.51 Å. Further analysis of these samples by the Greene–Kelley test confirmed them to be chiefly beidellite with a minor montmorillonite component (Table 1). It is therefore likely that most, if not all, of the miarolitic cavity smectite is beidellite.

Samples showing light yellow-brown to reddish brown colors are almost invariably smectite with a high percent expandability.

Illite

Illite is abundant in both soils and in miarolitic cavities (particularly cavities in the LGR, *e.g.*, Fig. 8); samples from miarolitic cavities composed predominantly of illite are brown to tan in color. Soil and miarolitic cavity samples may have very similar XRD patterns; however, the CTD profile of illite from miarolitic cavities is approximately lognormal (Fig. 9), with average thicknesses of crystallites of ~8.8 nm, whereas soil CTD values are asymptotic, with smaller mean thicknesses of crystallites ~5.8 nm (Fig. 10, Tables 1, 2). A plot of the mean of the log of crystallite thickness (α) and thickness variance (β^2) shows two distinctly separate populations, with cavity-formed illite having a smaller variance in thickness and larger mean thickness of crystallite, in contrast to a larger variance in thickness and smaller thickness for soil-generated illite (Fig. 11); as explained below, the miarolitic cavity illite that is non-lognormal is presumed to result from infiltration of soil illite and consequent mixing with cavity illite. Information regarding mechanisms of crystal growth can also be inferred from this plot. For example, superimposed on this graph are crystal-growth trajectories, based on modeling results from the recently developed computer program Galoper [Eberl *et al.* (1998b); see also Eberl *et al.* (2004) and references therein for recent applications of this program]. The leftmost line in this plot shows a theoretical crystal-growth trajectory for a continuous nucleation-and-growth mechanism, whereas the lower trajectory represents a mechanism of

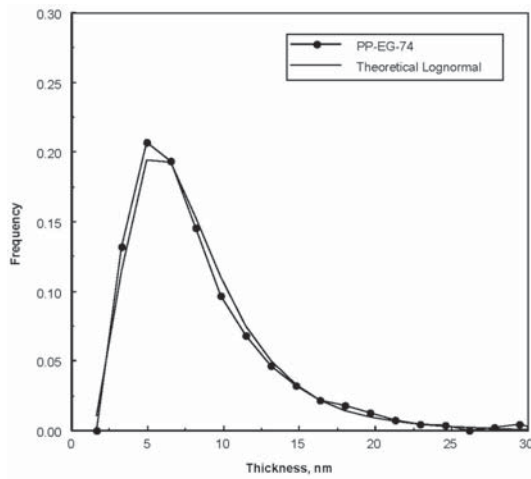


FIG. 4. CTD for the smectite (no. 74) shown in Figure 3, illustrating a lognormal distribution (dotted line). The solid line is the theoretical lognormal curve calculated from the same data.

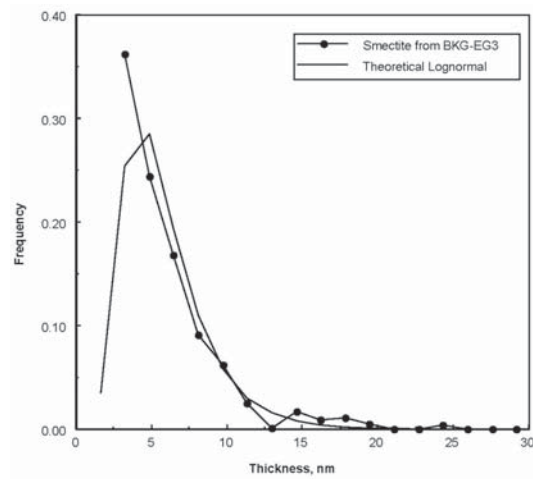


FIG. 6. CTD for smectite in soil sample BKG-3, illustrating a non-lognormal distribution (dotted line). The solid line is the theoretical lognormal curve calculated from the same data.

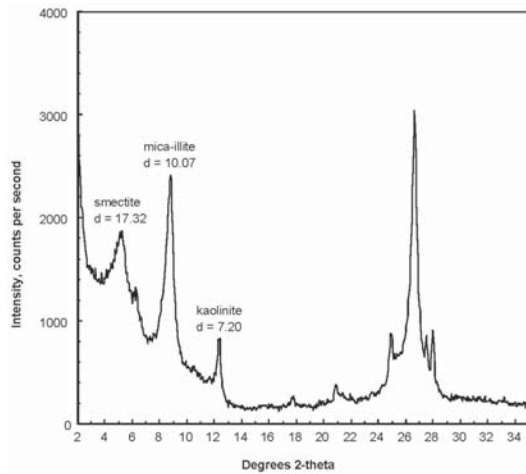


FIG. 5. XRD pattern of a glycolated, typical soil sample from the LGR (sample BKG-4), showing multiple clay minerals, *i.e.*, mixed-layer smectite-illite, illite, and kaolinite.

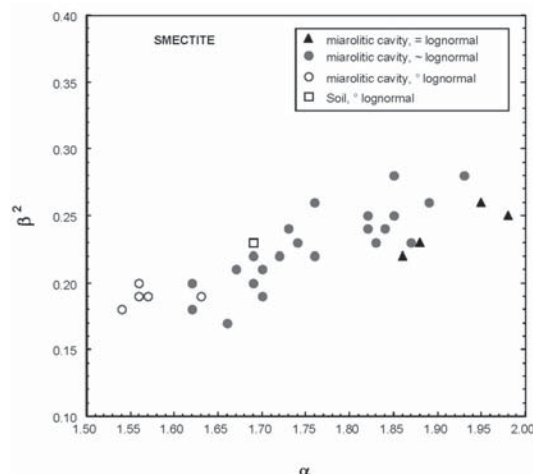


FIG. 7. Plot of the mean of the natural logarithms of crystallite thicknesses (α), and the variance of the natural logarithm of thickness (β^2), as calculated with the Galoper computer program, for both miarolitic cavity and soil smectite-bearing clay samples.

surface-limited growth without continuous nucleation. This plot accordingly shows the soil-derived illite to have a continuous nucleation and surface-controlled growth mechanism, in contrast to the mechanism for cavity-formed illite, which consists of a single or short-duration nucleation event followed by surface-

controlled growth without simultaneous nucleation. The mechanism for cavity-formed illite is suggestive of crystallization in a hydrothermal environment (and hence an authigenic origin), where levels of supersaturation are expected to diminish during crystallization. In contrast, for crystallization in the surrounding granitic

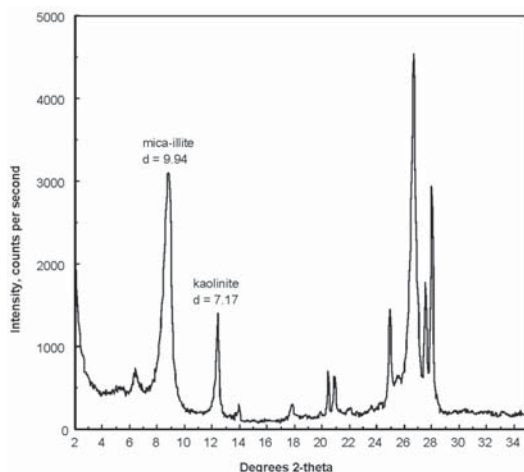


FIG. 8. XRD pattern of a miarolitic cavity illite (sample no. 15) from the LGR.

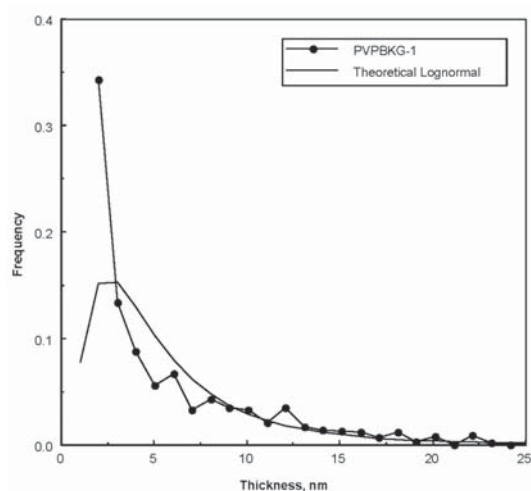


FIG. 10. CTD for soil sample BKG-1, illustrating a non-lognormal distribution for illite (dotted line). The solid line is the theoretical lognormal curve calculated from the same data.

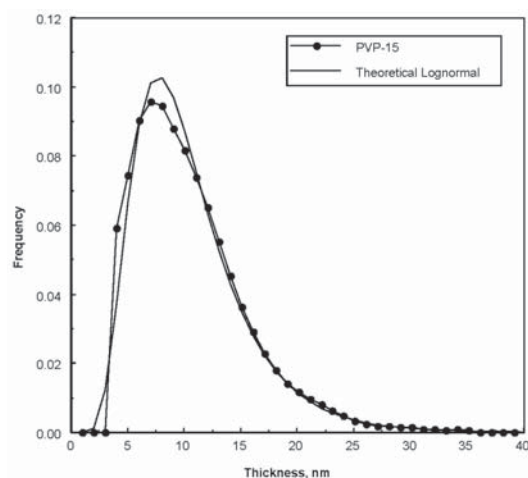


FIG. 9. CTD for the illite sample (no. 15) shown in Figure 8, illustrating a lognormal distribution (dotted line). The solid line is the theoretical lognormal curve calculated from the same data.

rock, continuing alteration of feldspar and a higher rock: water ratio would be expected to provide higher levels of mineral supersaturation and consequent continuous nucleation; this model of crystallization would be analogous to that hypothesized by Bove *et al.* (2002) for a hydrothermal system in the San Juan Mountains of Colorado. Thus, cavity and soil illites can be readily distinguished; cavity illite deviating from a lognormal shape and appearing at intermediate points on the α - β^2

plot is presumed to result from varying degrees of cavity weathering and consequent infiltration of soil illite.

Kaolinite

Kaolinite also is found in both cavities and soils, but seldom in substantial amounts in the soil; its relative absence in soils strongly suggests that it is authigenic where found as a predominant constituent within miarolitic cavities (*e.g.*, Fig. 12). Three samples of kaolinite show approximately lognormal CTDs (with some skew to the left; see Fig. 13), but most samples have CTD values that are distinctly not lognormal; an analysis of crystallite thickness shows a range in mean thickness of ~ 24 nm for lognormal samples to 10.7 nm for non-lognormal samples. Samples composed predominantly of kaolinite range in color from off-white to light brown.

DISTRIBUTION OF CLAY MINERALS IN THE PIKES PEAK BATHOLITH

Figure 14 shows the generalized regional distribution of the clay-mineral species in miarolitic cavities. No correlations are found between clay speciation and cavity mineralogy, size, or depth. However, on a basis of the above criteria for assessing provenance, some general correlations can be made pertaining to local and regional distributions of clay mineral species in miarolitic cavities. For example, on a regional scale, the occurrence of kaolinite appears to be governed by the nature of the host rock, indicated by its predominance in

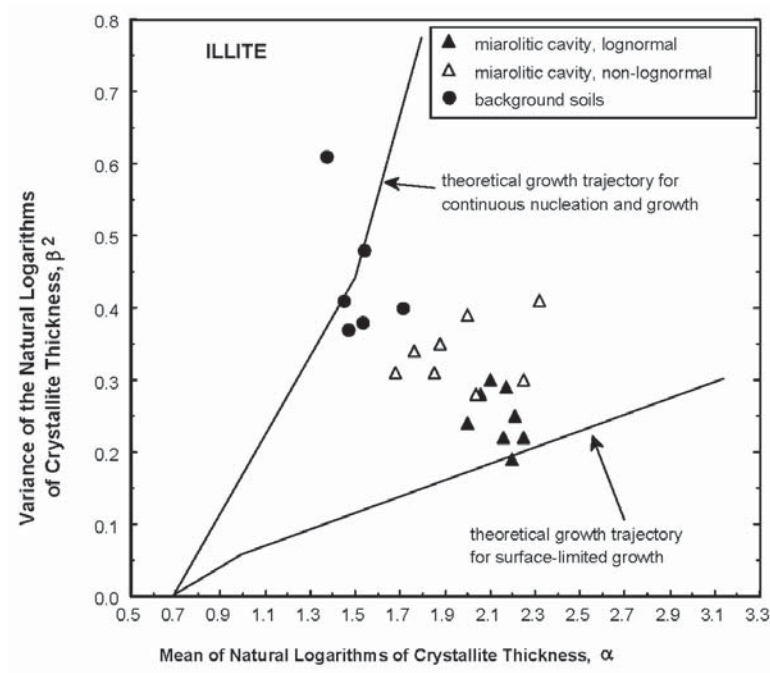


FIG. 11. Plot of the mean of the natural logarithms of crystallite thickness (α), and the variance of the natural logarithm of thickness (β^2), as calculated with the Galoper computer program, for illite-bearing clay samples from both miarolitic cavities and soil.

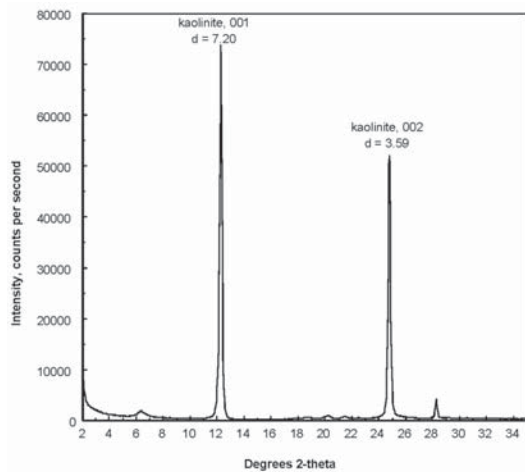


FIG. 12. XRD pattern of a miarolitic cavity kaolinite (sample no. 135) from the Sentinel Rock locality near Pikes Peak.

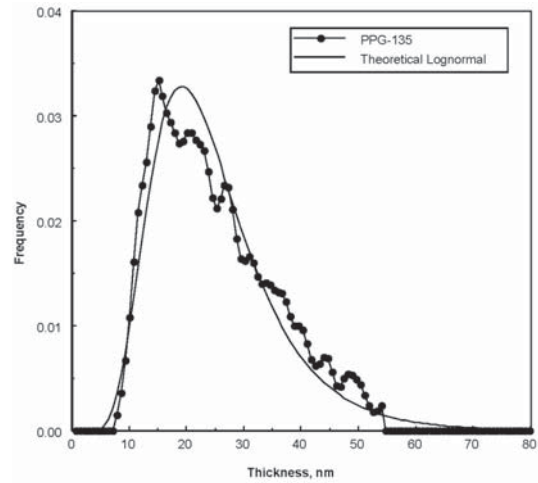


FIG. 13. CTD for the kaolinite sample (no. 135) shown in Figure 11, illustrating a near-lognormal distribution (dotted line). The solid line is the theoretical lognormal curve calculated from the same data.

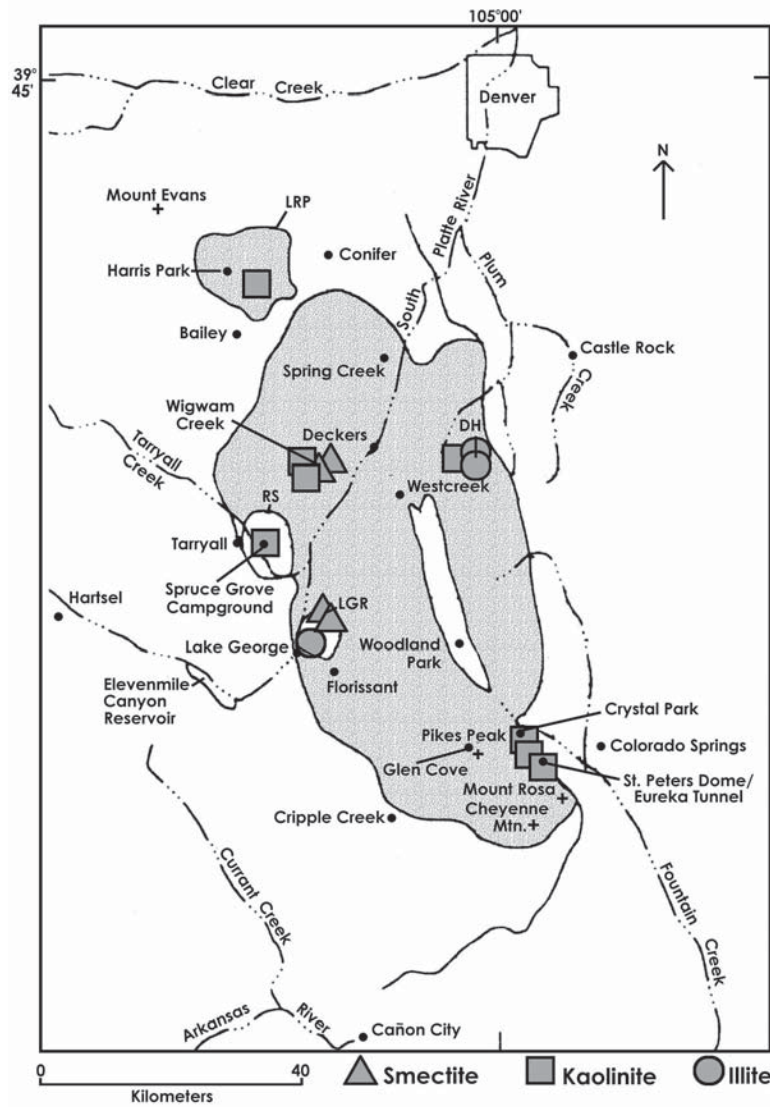


FIG. 14. Map showing the generalized regional distribution of clay minerals in the PPB; overlapping sites shown as a single point.

miarolitic cavities within highly evolved granitic rocks (*i.e.*, peraluminous compared to the Lake George ring complex). Such evolved rocks are F-rich, commonly topaz-bearing, and characterized by the presence of zinnwaldite that has a relatively low Fe content (and a correspondingly low index of refraction, n_{β}) or Fe-bearing muscovite (Kile & Foord 1998). These rock units include the Mt. Rosa Granite (St. Peters Dome, Sentinel Rock, and Eureka Tunnel), the Lone Rock Pluton (Harris Park), and the Redskin Granite (Spruce

Grove Campground). The prevalence of kaolinite in the more evolved granitic rocks is not unexpected considering that in such rocks, Si-bearing minerals are comparatively stable, thereby favoring hydrothermal solutions that are lower in Si^{4+} [*i.e.*, $\text{Si}(\text{OH})_4$] and in cation activities (*e.g.*, K^+ , Na^+), both of which factors increase kaolinite stability (Garrels & Christ 1965, Drever 1982). In contrast, only one sample from the LGR (of 39 total) shows principally kaolinite. Similarly, in a study of the orogenic, low-Fe granitic pegmatites in

San Diego County, California, Foord *et al.* (1986), noted that the formation of kaolinite represented a transition from an alkaline to an acidic (*i.e.*, more siliceous and less reactive) environment.

Local trends in clay mineralogy were also noted in this study, as evident in samples collected in or near the LGR. Smectite is more prevalent in the northern areas, whereas illite is more common in the southern areas of that complex (Fig. 15).

CONCLUSIONS

The heterogeneous nature and widespread pattern of clay-mineral occurrences within miarolitic cavities throughout the PPB are evidence that complex geochemical and physical processes influenced their formation. Analysis of XRD patterns permits an assessment of mineralogy and provenance based on expandability for smectite-group clays, and on the shapes of

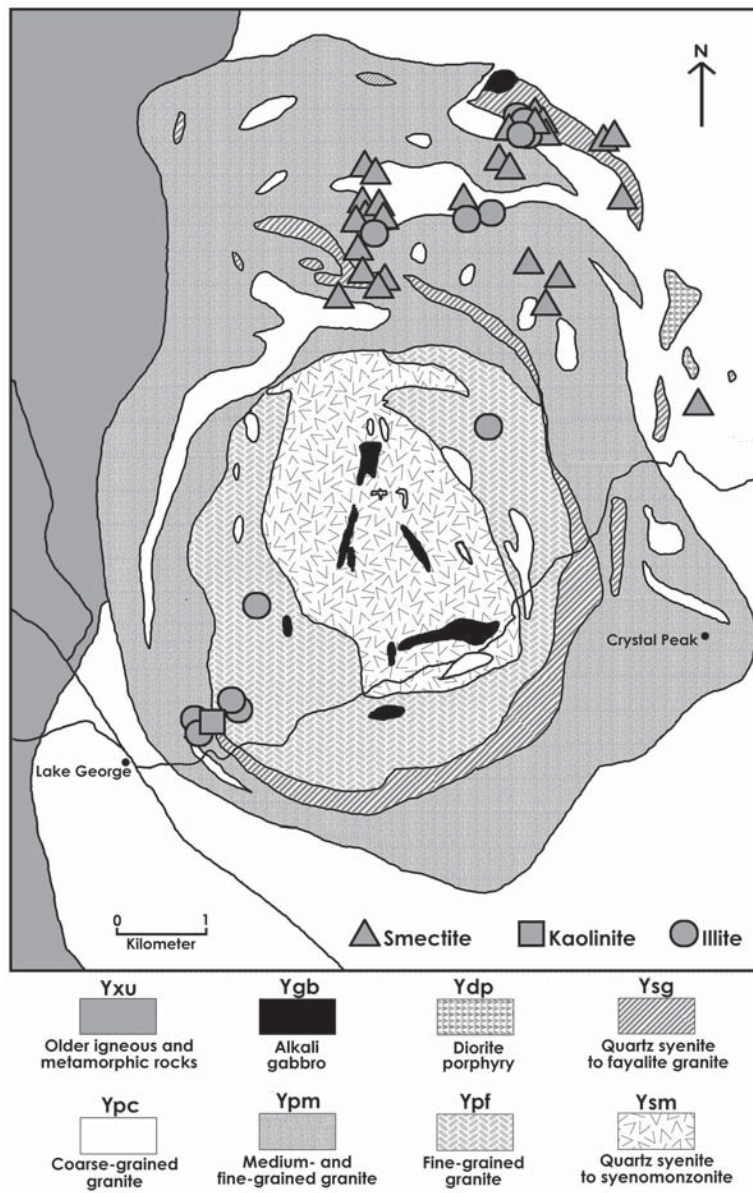


FIG. 15. Map showing approximate locations of monomineralic clay cavities in and near the LGR.

CTD profiles, crystallite-thickness variance, and mean thickness of illite crystallites. Authigenic illite shows a smaller variance in thickness and a larger mean thickness of crystallites than do their diagenetic soil-derived counterparts, and similarly, authigenic smectite shows larger mean crystallite thicknesses relative to soil-derived smectite. These observations provide a basis for determining provenance of the clays, and evidence for their neof ormation within miarolitic cavities. On the basis of these criteria, regional and local distributions of illite and smectite (beidellite) in miarolitic cavities can be determined; kaolinite is assumed to be authigenic where it is the predominant species in a given cavity.

Foord *et al.* (1986) noted the presence of both supergene and hypogene clays in pockets in the San Diego pegmatites. Likewise, in the present study, differences in CTD and mean thickness of crystallite are interpreted to be indicative of different origins, *i.e.*, hydrothermal and weathering processes. The hypogene, hydrothermally formed clays are presumed to be authigenic, whereas the diagenetically formed supergene clays are presumed to be allochthonous. Evidence to determine the source of the aluminosilicates during hydrothermal growth of the clays (*i.e.*, derived from alteration of surrounding feldspars or from residual aluminosilicates in solution) is not provided by the present results.

The lognormal CTD profile of clays within miarolitic cavities in the LGR indicates that initial growth of crystallites occurred according to surface-controlled, size-dependent growth kinetics, during which lognormal CTD shapes were established early in the crystallization history. A small β^2 for the illite CTD indicates rapid nucleation and subsequent surface-controlled growth, which constitute additional evidence for an authigenic, hydrothermal origin. Considerably more work will be necessary to further elucidate the factors governing the development and distribution of cavity clays in the pegmatites of the Pikes Peak batholith.

ACKNOWLEDGEMENTS

Dennis Eberl, Alex Blum, André Lalonde, and Pete Modreski reviewed this paper and provided valuable discussions and suggestions for improvement. Acknowledgement is given to Dianne Kile, who patiently assisted in collecting many of the samples used in this study. The use of trade, firm, or brand names in this paper is for informational purposes only and does not constitute endorsement by the U.S. Geological Survey.

REFERENCES

- BOVE, D.J., EBERL, D.D., MCCARTY, D.K. & MEEKER, G.P. (2002): Characterization and modeling of illite crystal particles and growth mechanisms in a zoned hydrothermal deposit, Lake City, Colorado. *Am. Mineral.* **87**, 1546-1556.
- BRINDLEY, G.W. (1980): Order-disorder in clay mineral structures. In *Crystal Structures of Clay Minerals and their X-Ray Identification* (G.W. Brindley & G. Brown, eds.). The Mineralogical Society, London, U.K. (Monogr. **5**, 125-196).
- DESBOROUGH, G.A., LUDINGTON, S.D. & SHARP, W.N. (1980): Redskin Granite: a rare-metal-rich Precambrian pluton, Colorado, USA. *Mineral. Mag.* **43**, 959-966.
- DREVER, J.I. (1997): *The Geochemistry of Natural Waters: Surface and Groundwater Environments*. Prentice Hall, Upper Saddle River, New Jersey.
- EBERL, D.D., DRITS, V.A. & ŚRODOŃ, J. (1998b): Deducing growth mechanisms for minerals from the shapes of crystal size distributions. *Am. J. Sci.* **298**, 499-533.
- _____, _____, _____ & NÜESCH, R. (1996): MudMaster, a program for calculating crystallite size distributions and strain from the shapes of X-ray diffraction peaks. *U.S. Geol. Surv., Open-File Rep.* **96-171**.
- _____, NÜESCH, R., SUCHA, V. & TSIPURSKY, S. (1998a): Measurement of fundamental illite particle thicknesses by X-ray diffraction using PVP-10 intercalation. *Clays Clay Minerals* **46**, 89-97.
- _____, ŚRODOŃ, J. & DRITS, V.A. (2004): Comment on "Evaluation of X-ray diffraction methods for determining the crystal growth mechanisms of clay minerals in mudstones, shales and slates," by L.N. Warr and D.L. Peacor. *Schweiz. Mineral. Petrogr. Mitt.* **83**, 349-358.
- FOORD, E.E., ČERNÝ, P., JACKSON, L.L., SHERMAN, D.M. & EBY, R.K. (1995): Mineralogical and geochemical evolution of micas from the miarolitic pegmatites of the anorogenic Pikes Peak batholith, Colorado. *Mineral. Petrol.* **55**, 1-26.
- _____, & MARTIN, R.F. (1979): Amazonite from the Pikes Peak batholith. *Mineral. Rec.* **10**, 373-384.
- _____, STARKEY, H.C. & TAGGART, J.E. (1986): Mineralogy and paragenesis of "pocket" clays in complex granitic pegmatites, San Diego County, California. *Am. Mineral.* **71**, 428-439.
- GARRELS, R.M. & CHRIST, C.H. (1965): *Solutions, Minerals, and Equilibria*. Freeman, Cooper & Co., San Francisco, California.
- HAWLEY, C.C. (1969): Geology and beryllium deposits of the Lake George (or Badger Flats) beryllium area, Park and Jefferson counties, Colorado. *U.S. Geol. Surv., Prof. Pap.* **608-A**.
- _____, & WOBUS, R.A. (1977): General geology and petrology of the Precambrian crystalline rocks, Park and Jefferson counties, Colorado. *U.S. Geol. Surv., Prof. Pap.* **608-B**.
- HUTCHINSON, R.M. (1976): Granite-tectonics of the Pikes Peak batholith, Colorado. In *Studies in Field Geology* (R.C. Epis

- & R.J. Weimer, eds.). *Colorado School of Mines, Prof. Contrib.* **8**, 32-43.
- _____ (1988): Granite-tectonics of the Pikes Peak batholith, Colorado. *In Field Trip Guidebook* (G.S. Holden, ed.). *Colorado School of Mines, Prof. Contrib.* **12**, 47-58.
- JAHNS, R.H. & WRIGHT, L.A. (1951): Gem- and lithium-bearing pegmatites of the Pala district, San Diego County, California. *Calif. Div. Mines, Spec. Rep.* **7-A**.
- KILE, D.E. & EBERL, D.D. (1999): Crystal growth mechanisms in miarolitic cavities of the Lake George ring complex and vicinity, Colorado. *Am. Mineral.* **84**, 718-724.
- _____ & FOORD, E.E. (1998): Micas from the Pikes Peak batholith and its cogenetic granitic pegmatites, Colorado: optical properties, composition, and correlation with pegmatite evolution. *Can. Mineral.* **36**, 463-482.
- LAUDERMILK, J.D. & WOODFORD, A.O. (1934): Secondary montmorillonite in a California pegmatite. *Am. Mineral.* **19**, 260-267.
- REYNOLDS, R.C. (1980): Interstratified clay minerals. *In Crystal Structures of Clay Minerals and their X-Ray Identification* (G.W. Brindley & G. Brown, eds.). Mineralogical Society, London, U.K. (Monogr. **5**, 249-303).
- SCHALLER, W.T. (1925): The genesis of lithium pegmatites. *Am. J. Sci.* **210**, 269-279.
- STARKEY, H.C., BLACKMON, P.D. & HAUFF, P.L. (1984): The routine mineralogical analyses of clay-bearing samples. *U.S. Geol. Surv., Bull.* **1563**.
- WOBUS, R.A. (1986): The Pikes Peak batholith and associated plutons. *In Colorado Pegmatites: Abstracts, Short Papers, and Field Guides from the Colorado Pegmatite Symposium* (P.J. Modreski, ed.). Colorado Chapter, Friends of Mineralogy, 70-71.
- _____ & ANDERSON, R.S. (1978): Petrology of the Precambrian intrusive center at Lake George, southern Front Range, Colorado. *U.S. Geol. Surv., J. Res.* **6**, 81-94.

Received December 15, 2003, revised manuscript accepted April 3, 2005.